JOURNAL OF GEOPHYSICAL RESEARCH: OCEANS, VOL. 118, 1–17, doi:10.1002/jgrc.20226, 2013

Entrainment-driven modulation of Southern Ocean mixed layer properties and sea ice variability in CMIP5 models

Sally E. Close[1] and Hugues Goosse[1]

Received 29 November 2012; revised 19 April 2013; accepted 1 May 2013.

[1] The evolution of the upper Southern Ocean hydrographic structure in response to the representative concentration pathways 4.5 (RCP 4.5) forcing scenario is analyzed using model data drawn from the coupled model intercomparison project phase 5 (CMIP5) archive. A robust freshening trend is evident, associated with an increase in stratification and decoupling of the upper ocean as the mixed layer gains buoyancy at a faster rate than the underlying ocean. The magnitudes of the individual terms of the salinity and heat budgets are evaluated. Convection-driven entrainment from the thermocline into the mixed layer is found to play a significant role in modulating the mixed layer salinity, whilst the heat budget of the mixed layer is dominated by a primary balance between atmospheric warming and the entrainment-modulated supply of oceanic heat from below the mixed layer. The relationship between oceanic heat storage below the mixed layer, ice thickness and atmospheric temperature is investigated, and a very disparate response noted amongst the models considered here. Based on this analysis, we hypothesize that the balance between the entrainment-modulated supply of oceanic heat from below the mixed layer and the heat supplied by the atmosphere may play an important role in determining the simulated sea ice variability.

Citation: Close, S. E., and H. Goosse (2013), Entrainment-driven modulation of Southern Ocean mixed layer properties and sea ice variability in CMIP5 models, *J. Geophys. Res. Oceans*, *118*, doi:10.1002/jgrc.20226.

1. Introduction

[2] The causes of recent variability in Antarctic sea ice coverage have been a source of considerable debate. Whilst the zonal-mean change in Antarctic sea ice extent has been relatively modest [*Zwally et al*., 2002; *Parkinson and Cavalieri*, 2012], this circumpolar picture masks complex and strongly varied regional patterns of variability (Figure 1), and contrasts strikingly with the Arctic region, where rapid and relatively uniform decreases in sea ice have been reported [e.g., *Comiso*, 2002, 2012]. In the Southern Ocean, increase in sea ice cover have been reported in the Ross [*Comiso et al*., 2011] and Weddell Seas [*Stammerjohn and Smith*, 1997], contrasting with a rapid decrease in sea ice in the Amundsen-Bellingshausen sector [*Stammerjohn et al*., 2012]. Whilst a number of theories have been proposed regarding likely driving mechanisms, including atmospheric temperature, wind stress, ocean temperature, and changes in precipitation [*Jacobs and Comiso*, 1997; *Liu et al*., 2004; *Liu and Curry*, 2010; *Manabe et al*., 1991; *Stammerjohn et al*., 2012; *Holland and Kwok*, 2012], with a particular emphasis placed on the interaction with the major atmospheric modes [*Simmonds and Jacka*, 1995; *Stammerjohn et al*., 2008; *Yuan and Li*, 2008; *Turner et al*., 2009], it has not yet been possible to fully explain recent Southern Ocean sea ice variability.

[3] The water masses formed in the Southern Ocean are exported globally and form a significant proportion of the global ocean volume. The formation of these water masses is tightly linked to climatic processes in the Antarctic region and the ocean, atmosphere, and cryosphere have all been suggested to have experienced significant variability in recent years. Between the 1950s and 2000s, the upper kilometer of the Southern Ocean is reported to have experienced a zonal-mean warming of ca. 0.17°C between 35 and −65°S [*Gille*, 2002, 2008], accompanied by a freshening tendency over the same depth range of approximately 0.04/yr in the thermocline to the north of the Polar Front [*Böning et al*., 2008]. At a regional scale, considerable variation has been observed, with an intense freshening tendency (ca., 0.1 between 1963 and 2000) throughout the water column in the Ross Sea [*Jacobs et al*., 2002] and an interdecadal warming tendency in the circumpolar deep water upwelled on to the West Antarctic Peninsula continental shelf [*Martinson et al*., 2008] and in warm deep water observed in the Weddell Sea [*Fahrbach et al*., 2011] being amongst the most substantial changes.

[4] The cryospheric and oceanic components of the climate system are strongly coupled: the brine rejection and heat loss associated with the sea ice formation cycle are

[1]Georges Lemaître Centre for Earth and Climate Research, Earth and Life Institute, Université catholique de Louvain, Louvain-la-Neuve, Belgium.

Corresponding author: S. E. Close, Centre de recherches sur la terre et le climat Georges Lemaître, Earth and Life Institute, Université catholique de Louvain, 1348 Louvain-la-Neuve, Belgium. (sally.close@uclouvain.be)

©2013. American Geophysical Union. All Rights Reserved.
2169-9275/13/10.1002/jgrc.20226

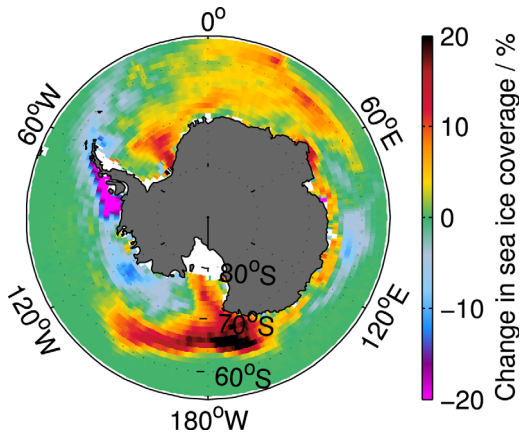

Figure 1. Thirty year change in sea ice coverage (%) over 1979–2009, derived from national snow and ice data center Nimbus-7 scanning multichannel microwave radiometer and defense meteorological satellite program F-13 special sensor microwave imager satellite data [*Cavalieri et al*., 1996].

instrumental in the formation of Antarctic bottom water, whilst the melting of sea ice in spring contributes to the seasonal freshening of the upper ocean mixed layer. Previous work has suggested that sea ice may contribute nontrivially to the ocean's response to future climate change, with *Bitz et al*. [2006] linking an enhanced freshening in the sea ice-covered region to weakening convection in the upper water column, and thus increased heat storage at depth. *Zhang* [2007] suggests that the increased stratification that results from the melting of sea ice, driven by atmospheric (and subsequent upper ocean) warming, may in fact be the cause of recent increases in Antarctic sea ice extent, with the associated suppression of convective overturning leading to a reduced supply of heat from the underlying ocean and in turn promoting further sea ice growth.

[5] In this work, we analyze experiments from the coupled model intercomparison project phase 5 (CMIP5) to further study the drivers of Southern Ocean mixed layer variability and the relationship to the sea ice that is formed there. In section 2, the processes governing mixed layer salinity and heat content are introduced, along with the CMIP5 models that are used in this study. Section 3 characterizes the evolution of mixed layer hydrographic properties in the CMIP5 projections and quantifies the contributions of the various components of the salinity and heat budgets to the long-term trend. The dominant mechanisms and their consistency with the corresponding changes in the sea ice system are then explored in section 4. We find a wide-scale decline in sea ice across the models to occur in conjunction with enhanced upper ocean stratification, caused by a freshening (and concomitant shoaling) of the mixed layer. South of 65°S, the long-term change in the salinity budget is found to be dominated by entrainment (i.e., changes in transport across the base of the mixed layer), with sea ice also playing a significant role in the near-continent region. The mixed layer heat budget indicates a primary balance between atmospheric warming and the entrainment-modulated supply of heat from the ocean underlying the mixed layer. The representations of the relative strengths of these processes are not consistent amongst the models studied here, and we suggest that this may be important in determining the skill with which models simulate sea ice processes.

2. Data and Methods

2.1. Data

[6] In this study, we employ data from seven models made available under the CMIP5 project (listed in Table 1), with the models selected based on availability of the variables necessary to quantify the various terms in the salinity budget. Since the number of ensemble members available for each of these models in the CMIP archive is not consistent, we analyze only one ensemble member from each model (r1i1p1) rather than the ensemble averages. Whilst the models utilized in this study employ sophisticated parameterizations of sub grid-scale eddy effects, they are not eddy resolving. We analyze a representative concentration pathways (RCP) 4.5 scenario, representing a medium mitigation situation [*Taylor et al*., 2011].

[7] Our aim in this work is to determine which processes are primarily responsible for driving mixed layer variability (with a particular emphasis on the ice-covered ocean) on interdecadal time scales under a forcing scenario similar to that of recent decades. The RCP4.5 scenario is hence chosen both due to its moderate strength external climate forcing and in order to provide a longer time series over which to study the interactions of the system than that afforded by the decadal experiments. The time scales of climate processes are often of multidecadal (or greater) length, and there is hence benefit in choosing an experiment with ~100 years of data (2006–2100), rather than the 30 years available from the satellite era to the present, so that the influence of decadal-scale oscillatory processes (e.g., the localized, extreme convective events that are evident in several of the models) is minimized.

2.2. Methods

2.2.1. Salinity Budget

[8] The variability in the salinity of the mixed layer may be estimated from the balance between evaporation,

Table 1. Details of Models From the CMIP5 Archive That Are Used in the Analysis

Modeling Center/Group	Model Name
Canadian Centre for Climate Modeling and Analysis	CanESM2
Centre National de Recherches Météorologiques/ Centre Européen de Recherche et Formation Avancées en Calcul Scientifique	CNRM-CM5
Commonwealth Scientific and Industrial Research Organization in collaboration with Queensland Climate Change Centre of Excellence	CSIRO-Mk3.6.0
NOAA Geophysical Fluid Dynamics Laboratory	GFDL-ESM2G
Institut Pierre-Simon Laplace	IPSL-CM5A-LR
Max Planck Institute for Meteorology	MPI-ESM-LR
Norwegian Climate Centre	NorESM1-M

precipitation, horizontal (Ekman, geostrophic and residual) advective fluxes, diffusive processes, vertical and lateral entrainment and brine/meltwater input from the sea ice formation cycle [e.g., *Dong et al.*, 2009; *Ren et al.*, 2011], described by:

$$\frac{\partial S_m}{\partial t} = \frac{(E-P)S_m}{h_m} - \mathbf{u}_e.\nabla S_m - \mathbf{u}.\nabla S_m + \kappa \nabla^2 S_m - \frac{w_e \Delta S_m}{h_m} - \frac{(\mathbf{u}.\nabla h_m)\Delta S_m}{h_m} - \frac{(\rho_i S_i - \rho_0 S_m)F_i}{\rho_0 h_m} \quad (1)$$

where S_m represents the salinity of the mixed layer. The mixed layer depth in this work is directly supplied as an output from the individual models' mixing schemes. (Comparison with mixed layer depth calculated by applying the criterion of *de Boyer Montégut et al.* [2004], which defines the mixed layer depth as the depth at which the potential density differs from the density at 10 dbar by 0.03 kg m^{-3}, to the same data indicates negligible difference between the two estimates, even in the presence of significant convection.) In the freshwater balance term, E denotes evaporation, P is precipitation, and h_m is the depth of the mixed layer. For horizontal advective processes, $\mathbf{u}_e$ represents the Ekman velocity, determined using:

$$\mathbf{u}_e = \frac{\boldsymbol{\tau} \times \mathbf{k}}{\rho_0 f h_m}$$

[9] where $\boldsymbol{\tau}$ is the wind stress, ρ_0 represents the characteristic density of the mixed layer (taken here to be 1027 kg m^{-3}) and f denotes the Coriolis parameter. $\mathbf{u}$ then indicates the non-Ekman, residual horizontal component of the velocity, obtained by subtracting the Ekman term from the model output velocity fields. Following *Dong et al.* [2009], the eddy diffusivity, κ, is held constant at 500 m^2 s^{-1}. (However, as in that study, and as detailed in section 3.2.3, our results are insensitive to the value chosen for κ.) In the entrainment term, w_e denotes the entrainment velocity at the base of the mixed layer, whilst ΔS_m is the salinity gradient across the base of the mixed layer (defined here as the difference between the mean mixed layer value and the salinity 10 m below the base of the mixed layer, and also employed in the estimate of lateral entrainment). Vertical velocity fields are not available for all of the models used in this study, and for consistency the entrainment velocity is thus estimated using:

$$w_e = \frac{\partial h_m}{\partial t} + w_{\mathrm{Ek}}$$

[10] where w_{Ek} is the Ekman pumping velocity, defined by:

$$w_{\mathrm{Ek}} = \nabla \times \frac{\boldsymbol{\tau}}{\rho_0 f}$$

[11] Comparison between the vertical velocity output available from models that directly provide this term and the entrainment velocity estimated using the above parameterization reveals negligible difference between the two representations, suggesting that the above estimation is sufficiently accurate for the purposes of this study. The sea ice contribution is estimated following *Watanabe et al.* [2004], where ρ_i is the density of sea ice (estimated to be 930 kg m^{-3}), S_i is the salinity of sea ice (estimated here as 5, following *Gough et al.* [2012]). F_i is the freshwater flux into the ocean due to cryospheric melt. Whilst some models do provide the freshwater flux due to sea ice melt as a direct output, again, this term is not widely available amongst the models considered here. We thus estimate F_i by subtracting the $(E-P)$ contribution from the total freshwater flux into the ocean, and applying a mask that sets the contribution to zero when there is no sea ice coverage (thus removing the residual contribution due to runoff at lower latitudes). The resulting freshwater flux includes contributions due to both sea ice melt and high-latitude runoff, which it is not possible to decompose further given the available data. With the exception of those variables explicitly defined as constants here, all values are supplied directly from output model fields. For ease of interpretation, unless otherwise stated, all figures depicting median properties are scaled to show the equivalent change of the variables over 50 years. We consider the Ekman transport component separately to other advective terms and, unless otherwise explicitly stated in the analysis, our use of the term "advective" in the following analysis refers to all horizontal advective processes other than Ekman transport.

2.2.2. Heat Budget

[12] The variability in the heat content of the mixed layer may be estimated from the balance between atmospheric forcing, horizontal (Ekman, geostrophic, and residual) advective fluxes, diffusive processes, vertical and lateral entrainment and heat extraction/input from the sea ice formation cycle [e.g., *Dong et al.*, 2007], described by:

$$\frac{\partial Q_m}{\partial t} = \frac{\partial Q_{\mathrm{atmos}}}{\partial t} - \mathbf{u}_e.\nabla(T_m \rho h_m)c_p - \mathbf{u}.\nabla(T_m \rho h_m)c_p + \kappa \nabla^2 (T_m \rho h_m)c_p - w_e \Delta T_m \rho c_p - (\mathbf{u}.\nabla h_m)\Delta T_m \rho c_p - L_i \Delta M_i \quad (2)$$

where Q_m represents the mixed layer heat content per unit area, and Q_{atmos} the heat supplied by the atmosphere per unit area. T_m denotes the mean temperature of the mixed layer and c_p is the specific heat capacity of sea water, taken here to be 3986 J kg^{-1} K^{-1}. ρ is the mean density of the mixed layer and ΔT_m represents the temperature gradient across the base of the mixed layer (as for salinity, this is defined here as the difference between the mean mixed layer value and the temperature 10 m below the base of the mixed layer). L_i is the latent heat of fusion of ice, taken here to be 2.93×10^5 J kg^{-1}, and M_i is the rate of change of sea ice mass per unit area, determined using the sea ice freshwater flux described in section 2.2.1. All other terms are defined as for the salinity budget. In considering sea ice, sufficient information is not available in the CMIP5 archive to calculate the contribution due to conduction, and we thus neglect this term in our analysis. As before, with the exception of variables defined as constants here, all values are supplied directly from model output fields.

3. Results

3.1. Evolution of Mixed Layer Properties

[13] The zonal-mean anomalies of mixed layer properties along the 65°S latitude band are shown in

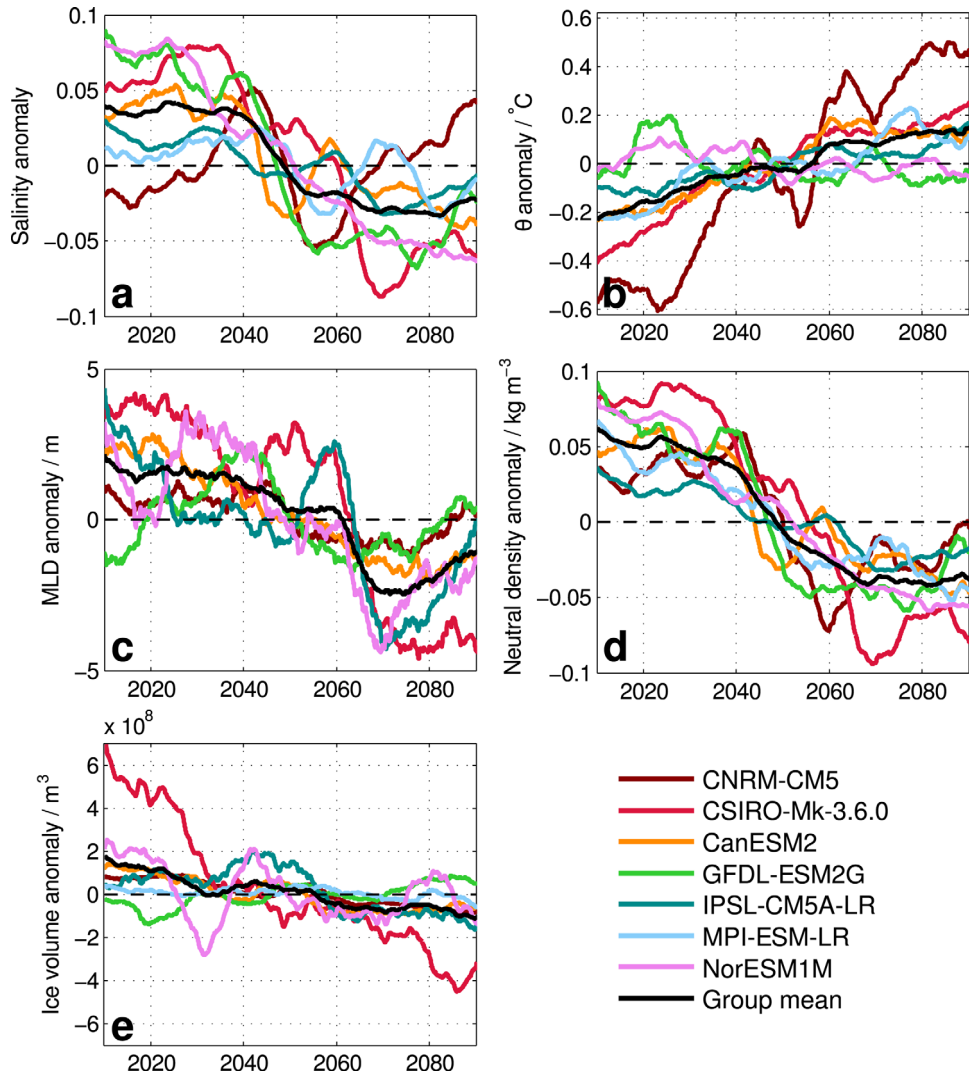

Figure 2. (a) Salinity, (b) temperature, (c) mixed layer depth, and (d) neutral density anomaly time series of mixed layer properties and (e) sea ice volume anomaly calculated as a zonal-mean average along the 65°S latitude band. Annual cycles are removed from all data, and the data smoothed with a 5 year moving average filter.

Figures 2a–2d. (This latitude is chosen here to demonstrate the evolution of the mixed layer in an area that experiences significant seasonal sea ice coverage, but still has an approximately circumpolar oceanic coverage, thus avoiding the bias toward the Ross and Weddell Seas that might be evident at higher latitudes.) With the exception of CNRM-CM5, a zonal-mean freshening tendency of O(0.1) over the 100 year period is evident in all models. Mixed layer temperature shows a less clear response: two of the models (GFDL-ESM2G and NorESM1-M) exhibit oscillatory behavior over the length of the time series, whilst four others (CanESM2, CSIRO-Mk3–6-0, MPI-ESM-LR, and IPSL-CM5A-LR) show a weak warming tendency. CNRM-CM5 again exhibits rather different behavior to the other models, showing a comparatively strong warming tendency, equating to a change of ~1°C over the period. All models exhibit a decrease in mean mixed layer neutral density over the period. The mean decrease is 0.12 kg m^{-3}, and, with the exception of CNRM-CM5, the change in buoyancy is predominantly driven by freshening. The temperature-driven density response of CNRM-CM5 is consistent with the freshwater-driven density response of the other models: the fluctuations in salinity in this model are accompanied by fluctuations in the temperature record that occur in a density compensating sense (though are not necessarily fully density compensating). The models thus demonstrate a reasonably consistent response in mixed layer density, showing both a similar magnitude and timing of change in all models, with the largest decreases in density occurring between 2030 and 2060.

[14] Throughout the projection, there is a tendency for MLD to shoal in the zonal mean of six of the seven models (with the seventh model, GFDL-ESM2G, exhibiting oscillatory behavior). MPI-ESM-LR simulates values of MLD that are many times the magnitude of those exhibited in other models in the region south of 45°S: over large areas, the winter mixed layer depth extends throughout the full depth of the water column (~4000 m), leading to a zonal

mean that is approximately 2 orders of magnitude larger than the mean of the other six models. For this reason, MPI-ESM-LR is excluded both from Figure 2c and from the group mean shown therein. Areas of full-column convection also occur in GFDL-ESM2G and CNRM-CM5. However, these areas are both localized and notably smaller than those in MPI-ESM-LR, and are excluded when calculating the zonal-mean MLD shown in Figure 2c to avoid aliasing the results. Sea ice volume declines in all models, again with the exception of GFDL-ESM2G, which displays oscillatory behavior, superimposed on a (nonrobust) increasing tendency. The model mean tendency implied by the zonal mean is therefore one of freshening, shoaling and buoyancy gain in the mixed layer, accompanied by a decrease in sea ice volume.

[15] As discussed previously, recent changes in Southern Ocean sea ice extent have been characterized by strong spatial variability, and we therefore now consider the homogeneity of the models' spatial response. Due to the small sample size and presence of extreme outliers in the model responses, we utilize the median and interquartile range, rather than the mean and standard deviation, to reduce any bias in the results. For all models and variables, the annual cycle is calculated by month and removed from the data prior to calculating the long-term tendencies.

[16] The median trend in mixed layer salinity, temperature, neutral density and depth anomaly of all the models examined here and their associated interquartile ranges are shown in Figure 3. The corresponding median trend/interquartile range for sea ice volume is also shown. Despite reasonable agreement amongst the models regarding the sign of the change, particularly in salinity (and hence also neutral density), the magnitude of the response is subject to large spatial disagreement. An examination of the individual models suggests that the spatial response in all properties is inconsistent amongst the set, with extreme values occurring in a number of models and in differing locations. The most robust features of the oceanic mixed layer property distributions are a wide-scale freshening (with large uncertainty in the magnitude of the response, despite agreement on the sign), a weak temperature response in the ice-covered area near the continent (with the disagreement in sign supporting the notion of an oscillatory response, as noted in the zonal mean) and a circumpolar tendency toward a reduction in density, with a spatial pattern almost identical to that seen in salinity in both the median trend and the interquartile range of the trends.

[17] The median trend in MLD anomaly and sea ice-volume anomaly are shown in Figures 3d and 3e, with the associated interquartile ranges shown in Figures 3i and 3j. The shoaling tendency suggested by the zonal-mean analysis is broadly replicated in Figure 3d, with the exception of the Bellingshausen Sea, where the trend is negligible. The uncertainty regarding the magnitude of the response is, however, again high, reflecting the intense localized areas of convection that occur in a number of models (as discussed above). These areas tend to occur in different areas in different models, thus leading to large patches of high uncertainty, such as that extending eastward out of the Weddell Sea.

[18] The development of the properties of the mixed layer relative to those of the underlying ocean is instructive in determining likely drivers of the freshening tendency noted here, and thus maps equivalent to those shown in Figures 3a–3c are shown in Figure 4, depicting the trend in the gradient of salinity, temperature and density across the base of the mixed layer. Over a large band extending eastward from the eastern Weddell Sea to the Amundsen Sea and spanning $\sim 60-70°$S, the Southern Ocean mixed layer freshens and gains buoyancy at a faster rate than the underlying ocean. The response of the temperature gradient is less clear, with little agreement amongst models over the sign of the change, and the spatial correspondence again implies that the increase in stratification is driven predominantly by the strong freshening of the mixed layer.

3.2. Contributions to the Salinity Budget

[19] The enhanced rate of change of salinity in the upper ocean relative to the underlying water column suggests that surface processes may play a significant role in driving this salinity change. The magnitude of the various terms of the salinity budget are thus estimated using the parameterization of equation (1), with the aim of qualifying the extent of influence of each term in driving the upper ocean change. All contributions are calculated directly using output fields from the CMIP5 models. The model median values for the various terms are shown in Figure 5, with the zonal means of the absolute individual model trends for the various terms of equation (1) also shown in Figure 6 for reference.

[20] The closure of the budget is estimated using the trend obtained from the sum of the terms of equation (1) and that obtained directly from the models' salinity output. Subtracting the trend of the summed terms from the trend of the model output, and averaging over the full Southern Ocean region analyzed here (south of 45°S), the mean difference between the two estimates of 50 year change in salinity for all models is 0.05 ± 0.07. The extent of closure varies amongst individual models. CNRM-CM5 and IPSL-CM5A-LR have the smallest residuals, with mean differences of 0.01 ± 0.03 and 0.00 ± 0.04 respectively over the region defined above. In contrast, CSIRO-Mk3.6.0 and GFDL-ESM2G both have rather large associated uncertainties, with mean differences of 0.09 ± 0.09 and 0.07 ± 0.09 respectively. For all of the models considered here, the residual is not a simple uniform over or underestimate, but exhibits spatial variability in the goodness of fit. In the case of CSIRO-Mk3.6.0, the closure at high latitudes is notably poor, with the mixed layer salinity exhibiting significantly greater freshening than that obtained from the sum of the terms evaluated here. Whilst the overall budgets hence close to within error, both for all individual models and for the model median, the error is nonetheless substantial, with the magnitude of discrepancy for the model median being $\sim 36\%$ of the total trend in mixed layer salinity. There are a number of possible sources for this residual error: equation (1) may not be an adequate description of certain terms of the budget, the definition (or estimation) of some of the variables employed here may not be optimal (e.g., $\Delta S_m, \kappa, h_m$), or terms that are missing from the budget (e.g., mixing) may affect the closure.

3.2.1. Evaporation-Precipitation Balance

[21] The median of the model trends in salinity due to changes in the E-P balance, scaled to show 50 years of

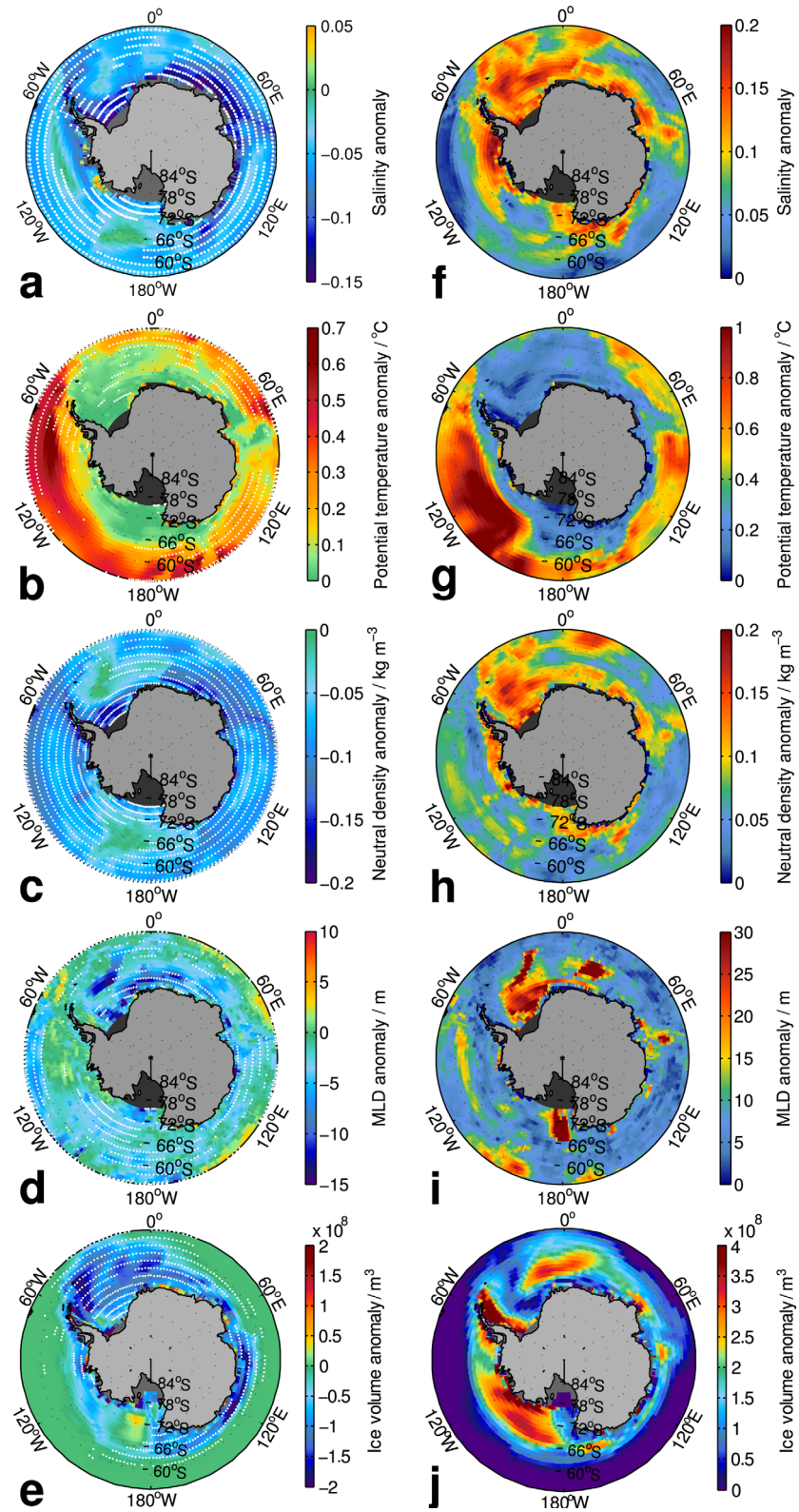

Figure 3. (a and f) Median/interquartile range of mixed layer salinity trends, (b and g) potential temperature trends and (c and h) neutral density trends over the period 2006–2100, scaled to show 50 year change. (d and i) The median/interquartile range of mixed layer depth trends, and (e and j) the same quantities for trends in sea ice volume, again over the period 2006–2100 and scaled to show 50 year change. White shading indicates areas where >75% of models agree on the sign of the trend.

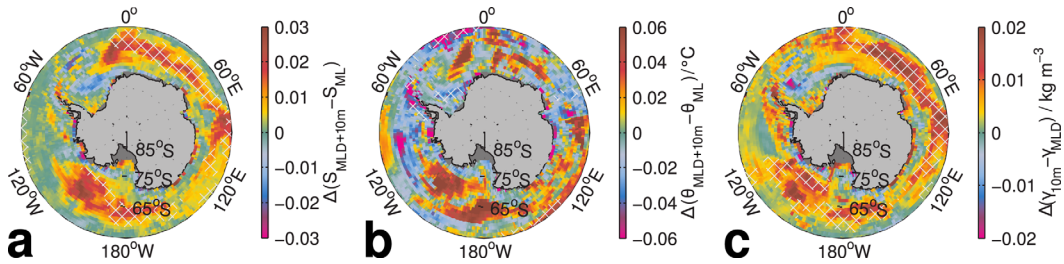

Figure 4. Median change in the gradient across the base of the mixed layer (defined as property value at a depth of MLD + 10m − property value in mixed layer) for (a) salinity, (b) potential temperature, (c) and density. The maps are scaled to show 50 year change. Gray hatching indicates areas where >75% of models agree on the sign of the trend.

change, is shown in Figure 5a. A widespread, robust freshening tendency is evident, with a zonal mean 50 year change of −0.024 over the range 60–75°S in the multimodel median (for comparison, the multimodel median zonal-mean mixed layer salinity change over the same latitude band is −0.06). Of all the terms considered here, the E-P contribution is perhaps the most consistently represented amongst the models (Figure 6); all seven models simulate a widespread freshening in response to changes in the E-P balance, and the multimodel interquartile range associated with this term is comparatively low ($\sim 5 \times 10^{-3}$). The median field obtained for this contribution is thus a relatively true representation of that produced by any individual model.

3.2.2. Advective Terms

[22] The model median contributions to the mixed layer salinity tendency by advective terms are shown in Figures 5b and 5c. In the median field, the magnitude of change explained by these processes is small in comparison to the long-term trend exhibited by the mixed layer salinity, with the change due to the combined advective terms accounting for only ∼12% (−0.004) of the total mixed layer salinity tendency (again, averaged zonally over the latitude range 60–75°S). However, considering the median of the absolute magnitudes of the relative trends, between 60–70°S the (total minus Ekman) advective and Ekman advection terms contribute a 50 year equivalent change of 0.053 and 0.047 respectively (evaluating the zonal mean of the absolute magnitudes). This suggests that, in magnitude, the non-Ekman and Ekman advective contributions are respectively the third and fourth largest contributors to the salinity budget over the 60–75°S latitude band, but that the spatial inhomogeneity in the model representations of these processes leads to cancellation between models that simulate freshening and salinifying contributions in overlying areas, thus masking the magnitude of these contributions. Both Ekman and non-Ekman advective fluxes hence appear to contribute nontrivially to the mixed layer salinity trend.

3.2.3. Eddy Diffusivity

[23] The median 50 year change in salinity due to eddy diffusion is shown in Figure 5d. The magnitude of the inferred contribution is substantially too small to contribute significantly to the long-term salinity change, with the total tendency being only ∼1% of the equivalent simulated mixed layer change. The largest magnitude changes occur along the Antarctic coastline. Nonetheless, even the largest changes are still O(2) smaller than the mixed layer tendency. The scale of difference between the changes inferred here and those simulated in the mixed layer are such that, as noted by *Dong et al.* [2009], the results are not sensitive to the choice of κ in the salinity equation to within reasonable constraints: using the value of $\kappa \sim 4000$ m^{2}s^{-1} suggested by *Sallée et al.* [2008] still suggests a contribution to zonal-mean salinity of O(1) smaller than that simulated in the mixed layer. Considering the absolute magnitude response, the contribution due to eddy diffusivity remains the smallest of the various terms: spatial inhomogeneity amongst the various models thus does not seem to significantly affect the interpretation. Eddy diffusivity may hence play a localized role in driving the long-term change in mixed layer salinity, both spatially, as suggested in this analysis, and possibly also temporally, since the time scales for this process may be shorter than the monthly resolution of the data employed here. However, the overall contribution to long-term salinity change appears to be negligible in the models analyzed here.

3.2.4. Sea Ice

[24] The inferred sea ice contribution to the decadal-scale mixed layer salinity trend is shown in Figure 5e. The pattern of change is spatially homogeneous, and is consistent with the decrease in sea ice suggested by the models, with a broad pattern of near-continent freshening under the sea ice, consistent with reduced brine rejection, accompanied by salinification at the ice edge, associated with reduced freshwater input from ice melt over time. The magnitude of change is largest in the near-continent region (south of ∼70°S) and, in certain localized regions, is independently of sufficient magnitude to explain the simulated mixed layer freshening. As for the advective terms, cancellation between positive and negative contributions due to spatial inhomogeneity does appear to diminish the relative magnitude of the contribution to the salinity budget due to sea ice in the median field. Considering the zonal median of the absolute magnitude of the sea ice contribution, this term is the second largest contributor to the salinity budget south of ∼60°S, having a median absolute magnitude of 0.058 over the range 60−75°S. In contrast, the median field obtained from the real model values suggests that sea ice contributes only 0.0059 to the salinity change. As for the advective terms, spatial disparity amongst the model simulations thus appears to significantly affect the interpretation of the relative role of sea ice in the salinity budget.

3.2.5. Entrainment

[25] The estimated change in salinity due to entrainment is shown in Figure 5f. A number of spatially coherent areas of change are again evident. In the near-continent region,

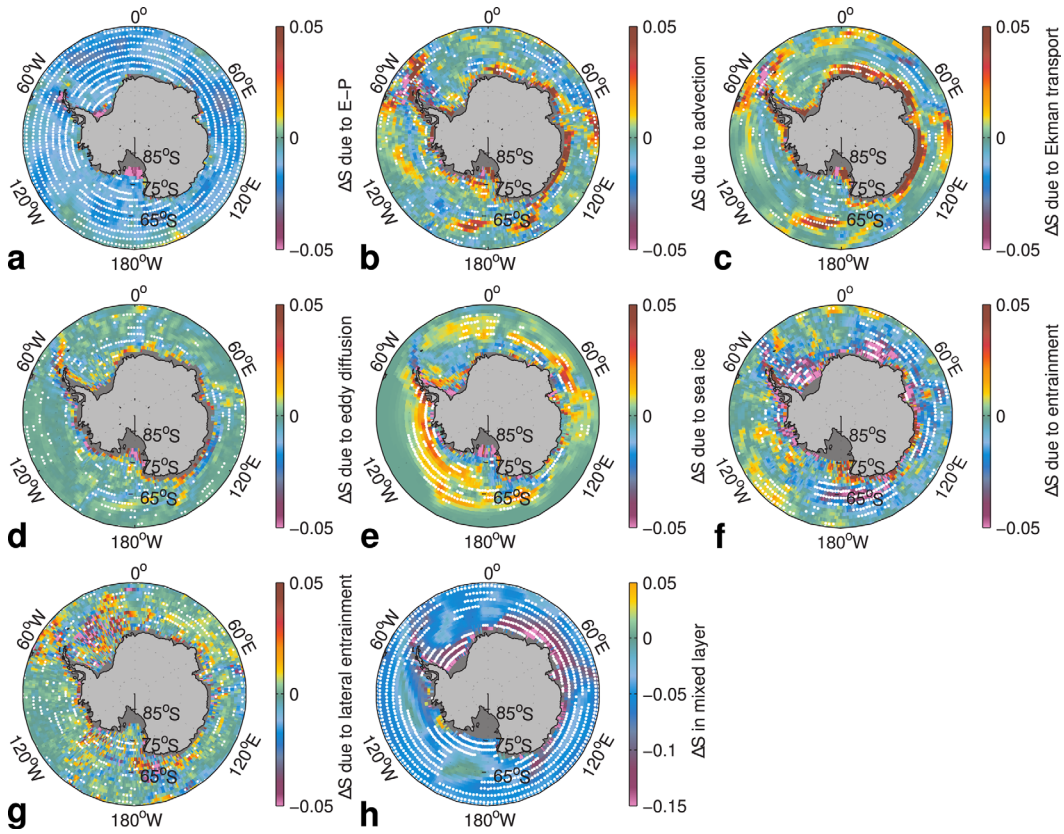

Figure 5. Median 50 year change in salinity derived from trends over the period 2006–2100 due to change in (a) evaporation-precipitation balance, (b) advection (excluding Ekman transports), (c) Ekman advection, (d) eddy diffusion, (e) sea ice, (f) entrainment, and (g) lateral entrainment. (h) The trend in mixed layer salinity. White shading indicates areas where >75% of models agree on the sign of the trend.

the tendency is primarily one of freshening. The contributions from this term are largest south of ~65°S, with the variability north of this region being both less spatially coherent and of notably smaller magnitude. In the median field, the mean change over the range 60−75°S is 0.030, accounting for 48% of the salinity tendency over this range. However, as for the advective and sea ice formation terms, the magnitude of the entrainment term in individual models is, on the whole, significant larger than this median value, and the term dominates the assessment based on absolute magnitude (Figure 6), supplying a mean contribution of 0.079 over the latitude range 60–75°S, decreasing from a maximum of 0.2 at 77°S to 0.096 at 70°S. The magnitude remains relatively constant over the range 70 − 65°S, having a mean value of 0.076, and decreasing in magnitude over the range 65−60°S to 0.017 at 60°S.

[26] The decomposition of the entrainment term into the contribution due to changes in MLD and that due to Ekman pumping (shown in Figure 6) demonstrates that the relative importance of the two terms is not consistent amongst the models examined here. Whilst the MLD contribution dominates in five of the models (CNRM-CM5, CanESM2, GFDL-ESM2G, IPSL-CM5A-LR and MPI-ESM-LR), particularly at high latitudes, CSIRO-Mk3.6.0 and NorESM1-M both experience a larger contribution from the Ekman-driven component. In contrast, at lower latitudes, the contributions of the two terms appear to be comparable, both for individual models and the group mean.

[27] The greater role of Ekman pumping in driving entrainment at high latitudes in CSIRO-Mk3.6.0 and NorESM1-M does not reflect an exceptionally large contribution from this term in either model, but rather a greatly reduced role of the MLD-driven component. Considering the MLD-driven entrainment component, whilst this covaries only weakly with either wind stress or wind stress curl in any given model, the rate of change of salinity due to this term shows strong correlation with the rate of change due to sea ice processes. In CNRM-CM5, CanESM2, GFDL-ESM2G, IPSL-CM5A-LR and MPI-ESM-LR this is evident as a strong positive correlation throughout the ice-covered area, with the correlation between the two anomaly fields lying in the range $0.6 \leq r \leq 0.8$ in all models. Whilst CSIRO-Mk3.6.0 and NorESM1-M also show strong correlation between the two fields, this is opposite in sign to that exhibited by the other models, and the strongest values are restricted to the ice edge. The differences in the sign of the correlation suggest that distinct physical mechanisms are dominant for the two cases. A possible interpretation for the positive correlation scenario is that increased ice melt freshens the mixed layer, driving an increase in stratification and concomitant decrease in entrainment as the mixed layer shoals, further amplifying the initial freshening

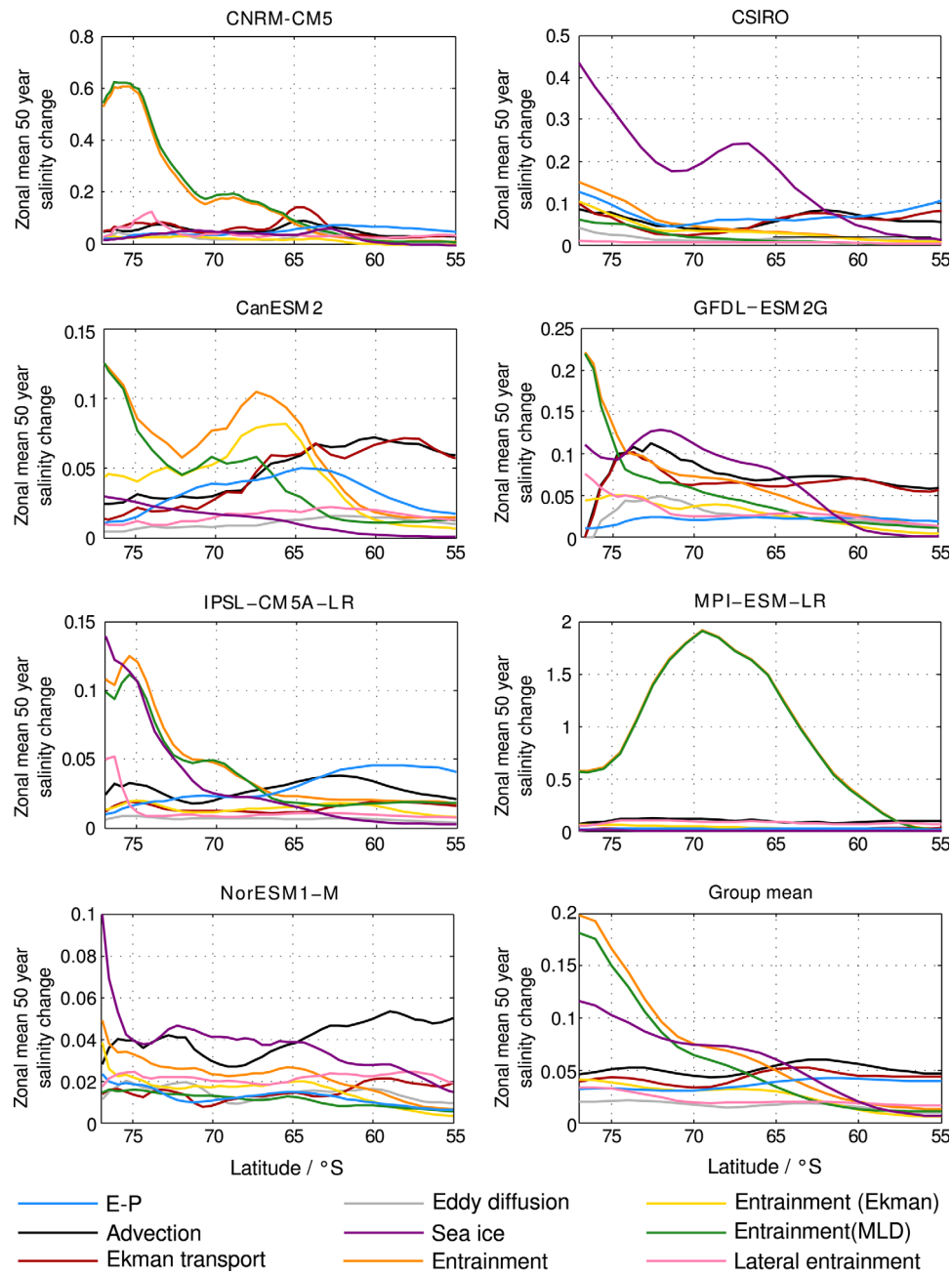

Figure 6. Zonal mean of absolute values of the trends for the various terms of the salinity budget for individual models. In addition to the total change due to entrainment, both the MLD-driven and Ekman-driven contributions to this term are also shown. MPI-ESM-LR is excluded from the group mean calculation because of the extreme values simulated in this model.

signal. In contrast, negative correlation may plausibly reflect a sequence of events such that increased ice melt permits enhanced air-sea heat transfer and thus increased (heat-driven) convection, driving a deepening of the mixed layer. The corresponding increase in entrainment would then drive a salinifying tendency, opposing the initial sea ice-driven freshening.

[28] The above correlations suggest that wind-driven effects play only a weak role in controlling the MLD-driven component of the entrainment term, and that changes in sea ice coverage and convective-driven changes in MLD are strongly linked. Whilst the MLD and both the zonal-wind stress and wind stress curl monthly anomaly fields are more strongly correlated in NorESM1-M at high latitudes than in any of the other models, with values of $r \sim 0.5$ south of 65°S, the same is not true of CSIRO-Mk3.6.0, which, similarly to the remaining five models, exhibits negligible correlation between these fields at high latitude. (CSIRO-Mk3.6.0 does, however, show a significantly weaker salinity gradient across the base of the mixed layer than the other models. The strength of the convective-driven component of the entrainment term thus appears to

be key to determining the high-latitude mixed layer salinity response to climatic forcing.

3.2.6. Lateral Entrainment

[29] The median 50 year change in salinity due to lateral entrainment is shown in Figure 5g. The model median response due to this term is both spatially inhomogeneous and of very small magnitude (the mean over the latitude range 60−75°S is $O(10^{-5})$). Considering the absolute magnitude response, lateral entrainment is the second smallest contributor to long-term salinity change, having a mean value of 0.018 over 60−75°S. As for the eddy diffusion term, whilst lateral entrainment may play a localized role in driving the long-term change in mixed layer salinity, the overall contribution thus appears to be negligible.

3.2.7. Mixed Layer Response

[30] For ease of comparison with the contributions of the individual terms, the total model median change in mixed layer salinity is shown in Figure 5h. As noted previously, a widespread freshening tendency is evident, with good agreement on the sign of the response amongst the models considered here. The largest decrease in salinity occurs in the near-continent region, with a zonal-mean freshening of 0.1 at 75°S, decreasing to 0.06 at 65°S and 0.05 at 60°S, and remaining approximately constant at this value to the north of this latitude within the study area.

[31] To briefly summarize the role of the various mechanisms contributing to the salinity budget: our analysis indicates that the largest magnitude controls on the high-latitude mixed layer salinity budget are entrainment and sea ice. The group mean shown in Figure 6 demonstrates the dominance of these terms at latitudes south of 65°S, with the reduction in entrainment being driven predominantly by the shoaling of the mixed layer depth. As discussed above, long-term changes in entrainment rate are strongly correlated with changes in sea ice thickness, but show little overall correspondence with changes in wind stress. Of the seven models considered, entrainment is the dominant process driving high-latitude salinity variability in five of these, with the other two (CSIRO-Mk3.6.0 and NorESM1-M) experiencing the greatest contribution from the sea ice term (Figure 6).

[32] The consistency with which the smaller magnitude terms are represented varies amongst the models. Changes in E-P are on the whole rather uniformly represented, with values in the approximate range 0.02−0.1 and comparatively weak meridional variation (with perhaps the exception of CanESM2 and IPSL-CM5A-LR, see Figure 6). The group mean shown in Figure 6 equally suggests the meridional variation of the advection term to be rather slight, with its increased importance north of ∼65°S owing to a decline in the magnitude of the entrainment and sea ice terms, rather than increases in the magnitude of the advective contribution. This pattern of increased importance of the advective term at lower latitudes is also evident in the individual models' behavior, again shown in Figure 6.

[33] In contrast with the preceding terms, the representation of the Ekman transport in the models is rather more varied. Whilst in several models, the magnitude and meridional variation closely match that of the advective term (notably in CNRM-CM5, CSIRO-Mk3.6.0, CanESM2, GFDL-ESM2G and the group mean), in NorESM1-M the magnitude of the Ekman transport term is only approximately half of that of the advective term. Equally, whilst IPSL-CM5A-LR, NorESM1-M and the group mean suggest relatively slight meridional variation in the magnitude of this term, in a number of models the magnitude is strongly latitude dependent. Examples of this are CanESM2, where the magnitude doubles between 70 and 60°S and CNRM-CM5, where a strong increase is evident at ∼65°S, coinciding with the overlying westerlies.

3.3. Contributions to the Heat Budget

[34] In the following section, the magnitude of the various terms of the heat budget are estimated using equation (2). All contributions are calculated directly using output fields from the CMIP5 models, and expressed as an equivalent change in monthly heat flux. The model median values for the various terms are shown in Figure 7, with the zonal means of the absolute individual model trends for the various terms below also shown in Figure 8 for reference.

[35] As for the salinity budget, the closure of the heat budget is assessed by subtracting the trend of the sum of the individual terms of the budget from the total mixed layer heat content change, and averaging over the full region analyzed here (south of 45°S). The model median field has a residual equivalent heat flux of 1.3±9.7 W m^{-2}, suggesting that the closure is reasonable, although the associated error is again fairly large. As for the salinity budget, the individual model response is rather varied. IPSL-CM5A-LR again has one of the smallest mean residuals, 1.4±6.1 W m^{-2}. GFDL-ESM2G also has a small mean residual (0.9±10.1 W m^{-2}); however, the error associated with this is large, representing significant localized spatial discrepancy. The greatest residual is associated with NorESM1-M, which has a mean value of 3.5±16.8 W m^{-2}. However, this is primarily reflective of poor closure in the lower latitudes, and south of 60°S the size of the residual is greatly reduced, having a mean value of 1.7±4.6 W m^{-2}. As for the salinity budget, the heat budgets for all models thus close to within error, but the associated error is large, having a magnitude of ∼31% of the mixed layer heat content trend of the median field. Possible sources of error are believed to be the same as those discussed previously for the salinity budget.

3.3.1. Atmospheric Forcing

[36] The change due to atmospheric forcing is shown in Figure 7a, and exhibits a spatially coherent response in the mixed layer heat content. The zonal-mean model median heat gain of 2.28 W m^{-2} over the 60−75°S latitude range is large within the context of the model median analysis, and suggests the atmospheric forcing to be the second largest driver of long-term change in this analysis. The absolute magnitude analysis similarly suggests a significant role of atmospheric forcing, where this is the third largest contributor to the budget, with a mean absolute value over the same latitude range of 3.55 W m^{-2}. The slight increase between the two estimates reflects the relatively consistent atmospheric response amongst the models. The zonal means for the individual models are shown in Figure 8 and confirm the similarity in both magnitude and spatial distribution amongst the models considered here.

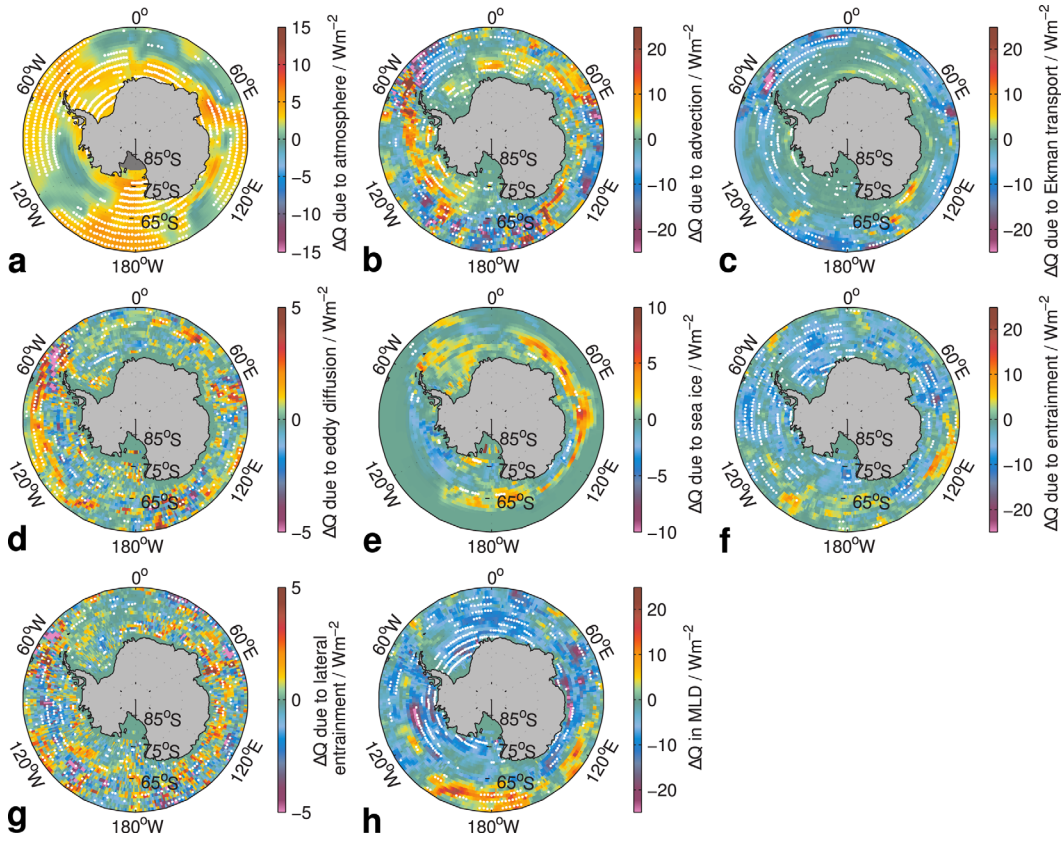

Figure 7. Median 50 year change in equivalent heat flux derived from trends over the period 2006–2100 due to change in (a) atmospheric forcing, (b) advection (excluding Ekman transport), (c) Ekman advection, (d) eddy diffusion, (e) sea ice processes, (f) entrainment, and (g) lateral entrainment. (h) The equivalent heat flux for the change in mixed layer heat content. White shading indicates areas where >75% of models agree on the sign of the trend.

3.3.2. Advective Terms

[37] The model median estimated changes in heat content due to advective terms are shown in Figures 7b and 7c. Whilst the overall pattern of spatial change is relatively inhomogeneous, coherent areas of change are evident. Such regions include an almost circumpolar band of heat gain in Figure 7b, centered at 65°S, and numerous smaller regions of heat loss to the north of this latitude. Figure 7c similarly reveals areas of coherent forcing in the Ekman contribution, with a circumpolar tendency of heat loss being evident to the north of 65°S, and negligible change to the south of this latitude. The model median suggests that, again considering the latitude range 60–75°S, advection (excluding the Ekman component) drives a weak zonal-mean heat gain equivalent to a change in heat flux of 0.18 W m^{-2} over a 50 year period, whilst Ekman transport drives a net heat loss of 0.34 W m^{-2}. However, the absolute magnitude estimate suggests that intermodel spatial cancellation in the median field again leads to an underestimate of the magnitude of change, yielding a mean change in equivalent heat flux of 5.37 and 2.34 W m^{-2} for the advective and Ekman terms (Figure 8), and suggesting them to be the largest and fourth largest drivers of long-term heat content change respectively.

3.3.3. Eddy Diffusion

[38] As for the salinity budget analysis, eddy diffusion does not appear to contribute strongly to the long-term trend in mixed layer heat content. Whilst areas of coherent spatial change are evident in the model median (Figure 7d), such as the bands of heat gain and loss that extend from 60 – 120°W, these features are of very small magnitude in comparison to the remaining terms of the budget. The zonal-mean average over 60–75°S of the model median term indicates a heat gain of 0.03 W m^{-2} driven by eddy diffusion over this latitude range, whilst the absolute magnitude estimate over the same area implies a change of 1.31 W m^{-2}.

3.3.4. Sea Ice

[39] The trend due to changes in the heat expended in forming/melting sea ice are shown in Figure 7e. The pattern of change shows a band of increased equivalent heat flux stretching from 0 to 210°W, suggesting increased expenditure of heat in melting sea ice at the ice edge, accompanied by a decreasing heat flux tendency adjacent to the continent. The contribution to the total budget due to this term is comparatively small, both in the real median and absolute magnitude estimates, having mean values of 0.59 and 1.62 W m^{-2}, respectively over the latitude range 60 – 75°S.

3.3.5. Entrainment

[40] The model median change in mixed layer heat due to entrainment is shown in Figure 7f. An overall trend of heat loss is indicated, with good agreement on the sign of

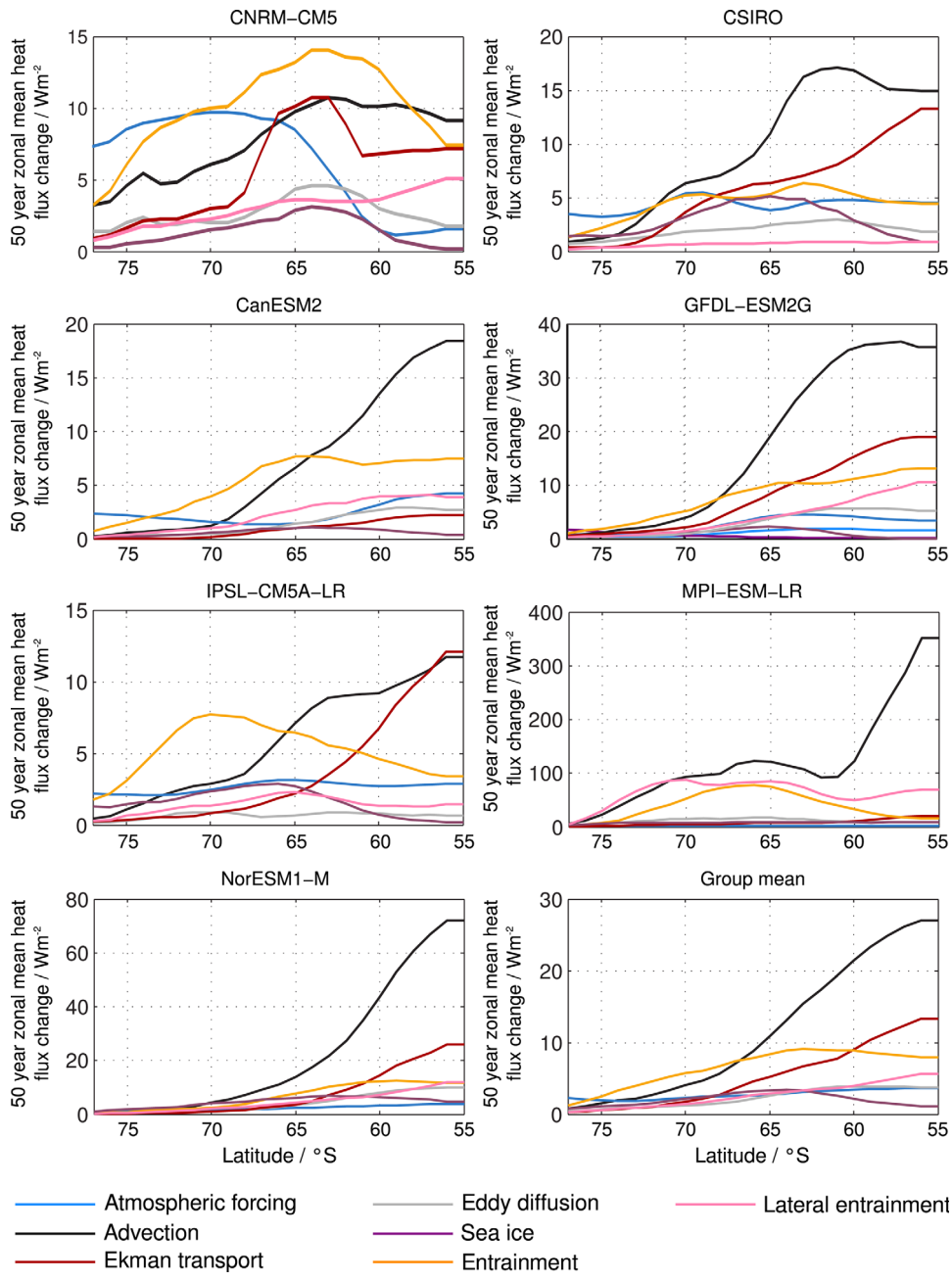

Figure 8. Zonal mean of absolute values of the trends for the various terms of the heat budget for individual models. MPI-ESM-LR is excluded from the group mean calculation because of the extreme values simulated in this model.

the change amongst the various models. The model median field shows a mean tendency of -2.37 W m^{-2} over the range 60−75°S, making this term the largest contributor to changes in heat content in the median field. Considering the absolute magnitude estimate, over the same latitude range the entrainment term contributes 4.26 W m^{-2}, suggesting this term to be the second largest magnitude driver of the long-term change in heat content over this latitude range.

3.3.6. Lateral Entrainment

[41] The model median change in mixed layer heat content due to lateral entrainment is depicted in Figure 7g. As for the eddy diffusivity term, the spatial patterns of change are less coherent than for the remaining terms of the budget, and the magnitude of change is also comparatively small. Over the 60−75°S latitude range, the model median field indicates that lateral entrainment drives the smallest contribution to the mixed layer heat content change, having a mean value of 0.06 W m^{-2} over this latitude range, increasing to 1.37 W m^{-2} in the absolute magnitude analysis. An examination of individual models shows that the colocation of areas of heat gain and loss on the same latitude parallel acts to reduce the magnitude of the zonal mean. However, the magnitude of lateral entrainment-

driven heat gain/loss in the coherent areas of change is low in all models (except MPI-ESM-LR, which exhibits persistent deep convection). It thus appears that the lateral entrainment-driven contribution to mixed layer heat content change is low both locally and in the overall picture.

3.3.7. Mixed Layer Response

[42] The total model median change in mixed layer heat content is shown in Figure 7h, and reveals an overall decrease in heat content. This response contrasts with the weak change in temperature evident in the mixed layer temperature trend analysis discussed previously (see Figure 3b), and indicates that the decrease in high-latitude mixed layer heat content reflects a decrease in mixed layer volume (i.e., shoaling of the mixed layer depth) rather than a decrease in temperature. Over the latitude range 60−75°S, the mixed layer exhibits a mean heat loss equivalent to 4.02 W m^{-2} in the model median field, with the absolute magnitude estimate indicating a change of 7.76 W m^{-2} over the same latitude range.

[43] In summary, the above analysis suggests that the high-latitude mixed layer heat content change is primarily determined by a balance between entrainment and atmospheric forcing. North of ~68°S, advection increases steadily, and rapidly becomes the largest magnitude contributor in the majority of the models (see Figure 8). However, the magnitude of the contribution due to advection varies strongly amongst the models, with extreme values simulated by NorESM1-M (~75 W m^{-2} at 55°S) and MPI-ESM-LR, but a rather weak contribution in CNRM-CM5 (~9 W m^{-2} at 55°S–approximately eight times smaller than NorESM1-M).

[44] A number of features of the heat budget show contrast with that of the salinity budget. In all models, the Ekman transport contribution shows a general tendency to increase northward in the heat budget, contrasting with the salinity budget, where there is no overall tendency in the group mean (Figure 8). This distribution reflects the trends in mixed layer temperature noted previously (Figure 3b), where the contrast between high- and low-latitude trends are much more striking than those evident in the salinity field.

[45] A further contrasting aspect of the heat budget analysis concerns the smaller magnitude terms: Figure 8 suggests that the relative magnitudes of the sea ice, lateral entrainment and eddy diffusion terms are more varied amongst the models here than in the salinity analysis. Whilst for the majority of the models, the contribution to the heat budget from sea ice processes is small at all latitudes, in NorESM1-M this term provides the largest magnitude contribution to heat content change in the region to the south of ~70°S, providing a contribution of similar magnitude to that of entrainment and atmospheric heating. The varying importance of the sea ice, lateral entrainment and eddy diffusion terms amongst the three models is reflected in the group mean, shown in Figure 8, in which the magnitude of these three terms is similar. However, there is some suggestion that lateral entrainment increases in importance further north, with this term increasing in magnitude with latitude in four of the models (CNRM-CM5, CanESM2, GFDL-ESM2G, and NorESM1-M), and thus also in the group mean.

4. Discussion

4.1. Salinity and Heat Budgets

[46] The CMIP5 models considered in this analysis demonstrate a robust mixed layer freshening tendency in the RCP4.5 scenario, accompanied by little concomitant change in temperature, a salinity-driven reduction in neutral density, and a shoaling of the mixed layer depth. Broadly, ice volume is projected to decrease. The freshening of the mixed layer occurs at a faster rate than that of the underlying ocean, suggesting a gradual decoupling of the mixed layer (previously noted by *Sen Gupta et al*. [2009] and *Capotondi et al*. [2012] in analyses based on CMIP3 models) as the mixed layer becomes increasingly less dense.

[47] The analysis of the relative magnitudes of the various terms of the salinity budget reveals a very spatially disparate portrayal of the importance of the various contributions to the overall mixed layer salinity tendency. Whilst, in magnitude, the entrainment-driven contribution dominates the budget at latitudes south of ~65°S, the colocation of areas of freshening and salinification in the various models leads to a reduced magnitude estimate in the median field. In contrast, the uniform freshening yielded by the E-P term (Figure 5a) suggests a rather coherent contribution to the salinity budget. Given its uniform distribution, the E-P term might thus be expected to account for a significant proportion of the variability. However, the median absolute magnitude of this contribution is approximately half that of the contribution due to advection, and a third of that due to entrainment over the area to the south of ~65°S. The response that is most consistently simulated by the models is thus not necessarily that which makes the greatest contribution to the salinity budget, with rather the uniformity of the response creating a median field which closely resembles that of any given model.

[48] The salinity budget south of 60°S appears to be dominated by the contribution due to entrainment. As discussed previously in section 3.2.5, the strong correlations between the $\partial h_m/\partial t$ and $\partial S(\text{sea ice})/\partial t$ anomaly time series suggest this to be driven predominantly by convection associated with the sea ice formation cycle, with forcing due to changes in wind stress playing a much smaller role. Sea ice processes provide a further significant contribution, particularly in the near-continent region (south of ~65°S), with advective terms also contributing significantly, becoming the dominant driver of the mixed layer salinity tendency north of ~65°S. Whilst the entrainment term is implied to dominate the long-term mixed layer salinity response, these changes in entrainment rate cannot occur in isolation: an initial driver is required. This suggests a crucial role of the smaller magnitude terms in initiating these changes in entrainment. It is thus plausible that enhanced sea ice melt or changes in the evaporation-precipitation balance drive an initial freshening of the mixed layer, leading to an increase in stratification and shoaling of the mixed layer. The associated reduction in $\partial h_m/\partial t$, suggested by our analysis to be the dominant control on entrainment in most of the models, would decrease the amount of heat made available to the mixed layer from below the thermocline, in turn promoting further sea ice growth, as discussed previously by *Zhang* [2007]. In the absence of external

forcing, the brine rejection associated with this increased sea ice formation rate would promote an increase in entrainment rate, counteracting the above cycle of events. However, persistent changes in the E-P balance may act here to maintain the increased stratification, or, equally, increased atmospheric heating may increase the buoyancy of the mixed layer either through heating or through melting sea ice, supplying additional freshwater to the upper ocean. In the presence of external forcing, it is hence possible that an initial forcing of comparatively small magnitude may be amplified by changes in entrainment rate.

[49] The absolute magnitude analysis suggests that the high-latitude mixed layer heat budget experiences the greatest contribution from the advective, atmospheric forcing and entrainment terms. Of these terms, entrainment provides the most spatially coherent cooling contribution, whilst atmospheric forcing provides the only spatially coherent heating contribution of any of the terms in the heat budget. Visually, the model median mixed layer heat content trend bears perhaps the greatest resemblance to the entrainment response. An analysis of the proportion of variance explained by the various terms contributing to the heat budget confirms this: entrainment and atmospheric heating terms in combination describe the greatest proportion of the heat content change observed in the mixed layer, explaining 37% and 20% of the observed spatial pattern of variance in the median field over the full study region respectively when considered independently, and 45% when considered in combination. In contrast, advection explains only 5% of the observed variance, whilst the remaining terms explain less than 1% of the variance. None of these remaining terms act to increase the proportion of variance explained if combined with the entrainment and atmospheric terms. This analysis thus hints at a primary large-scale balance between an entrainment-driven cooling, linked to a reduced supply of upwelled oceanic heat, and atmospheric warming in determining the mixed layer heat content. The poor spatial correlation notwithstanding, the magnitude of the advective term suggests that this may contribute significantly at local scales; however, the incoherent spatial distribution implies that this term does not set the large-scale mixed layer response.

[50] The dominance of the sea ice and entrainment contributions noted above appears to be corroborated by the mixed layer salinity and temperature change portrayed in Figures 3a and 3b: as the mixed layer freshens, the density gradient across the base of the mixed layer increases, leading to a decrease in the entrainment rate as convection weakens, and thus a reduction in the volume of saltier water entrained from below. As the mixed layer decouples, the enhanced upper ocean stratification acts to suppress convective overturning, thus leading to a decrease in upwelled ocean heat flux. The significant role of entrainment implied by the heat budget analysis provides further support for this picture, suggesting that the reduction in entrainment at high latitudes (south of ~67°S, see Figure 8) may be important in limiting the temperature increase of the mixed layer, compared to the warming evident in the extrapolar region.

[51] The enhancement of upper ocean stratification, suppression of convective overturning and associated decrease in upwelled oceanic heat flux has previously been suggested by *Zhang* [2007], amongst others, as a potential mechanism by which the rate of sea ice melt might be limited, thus providing a potential explanation for the increases in Antarctic sea ice coverage reported in recent decades. In the following section, we thus present an exploratory analysis of the links between the sea ice coverage simulated by the models and their representations of entrainment.

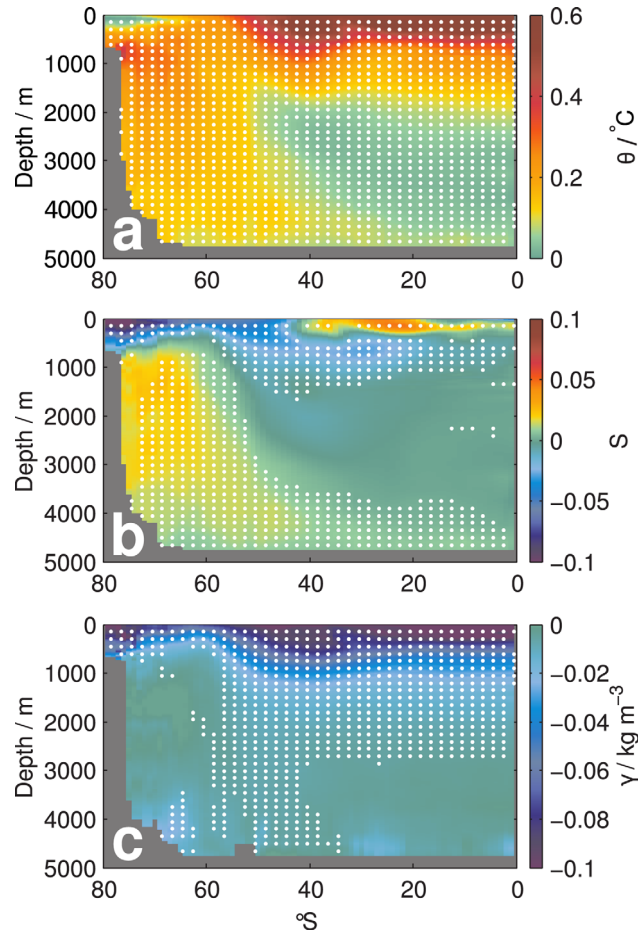

Figure 9. 50 year change in (a) potential temperature, (b) salinity, and (c) neutral density calculated from the trend on isobathic surfaces in the ocean interior over the period 2006–2100. White shading indicates areas where >75% of models agree on the sign of the trend.

4.2. Links to Sea Ice Variability

[52] The structure of changes occurring in the ocean interior are consistent with the above notion that the sea ice coverage is modulated by a balance between downwelled heat supplied by the atmosphere and upwelled oceanic heat. The model ensemble mean of the zonal means of potential temperature, salinity and density are shown in Figure 9. The strongest high-latitude freshening signal occurs in the top 500 m of the water column to the south of ~70°S. The magnitude is greatest at the highest latitudes (equivalent to ~0.11 over 50 years), and decreases as the anomaly is advected northward and subducted into the interior (~0.02 upon subduction at 50°S), consistent with a significant influence of reduced brine rejection and weakened entrainment in driving the high-latitude freshening signal,

which is then advected northward across the Antarctic Circumpolar Current. Below this area of freshening, an underlying area of (less intense) salinification is evident to the south of ~55°S, extending over most of the water column from below the area of freshening to a depth of ~4500 m. This salinification occurs concomitantly with an increase in temperature of ~0.2°C, and has little associated signature in density, suggesting that this increase is not forced by surface processes, but rather linked to dynamical changes.

[53] Increases in heat storage at depth may be induced by a number of processes (e.g., adiabatic movement of water masses). Similarly, sea ice coverage may be influenced by a variety of mechanisms, including, for example, atmospheric heating, changes in wind stress, and changes in heat supply from the ocean. Within the scope of this study, it has not been possible to analyze fully either the causes of the increased heat storage at depth noted in the models here, or all of the factors that may influence sea ice variability, and we thus stress the limitation that the following analysis does not consider the full range of mechanisms that may drive either sea ice or deep ocean heat storage variability. Nonetheless, the mixed layer heat budget analysis above suggests that, in the majority of models considered here, convection-driven entrainment is the primary control on the supply of upwelled oceanic heat to the mixed layer, and thus it is plausible that this mechanism may also be of importance in influencing both sea ice coverage and the heat stored at depth. Increased heat storage at depth associated with a weakening of convection has been noted in a number of previous studies [*Manabe et al.*, 1991; *Gregory*, 2000; *Huang et al.*, 2003; *Bitz et al.*, 2006], and both the strong dependence of entrainment on convective processes noted above and the meridional limitation of the deep warming tendency to the ice-covered area further support the suggestion of *Bitz et al.* [2006] that the weakening of convection in this region is related to sea ice processes.

[54] The relative dependence of ice thickness on heat storage at depth and on surface air temperature is assessed by performing a multiple-linear regression (of the form $\Delta(\text{ice}) = a + b\Delta(\text{heat storage}) + c\Delta(\text{atmospheric temperature})$, where a,b, and c are constants) for each of the models. Heat storage at depth is quantified by evaluating the mean potential temperature anomaly (relative to the full-period monthly means) over the depth range 500–1000 m. (Anomalies relative to the full-period monthly means are similarly employed for both surface air temperature and ice thickness. Whilst a similar relationship holds for sea ice extent to that found for ice thickness, ice thickness is preferred here as a diagnostic because it provides a truer representation of the heat capacity of the ice.) The full 100 year period is split into 20 subperiods of 5 year length, and for each time period the relationship between reconstructed ice thickness anomaly, mean potential temperature anomaly at depth and surface air temperature anomaly is quantified. By splitting the full period into shorter time intervals, a greater number of sample points are created, thus permitting an evaluation over varying conditions and providing a more representative overview of the relationships between the variables. The variance inflation factor for the three variables considered here is low, suggesting that multicollinearity is negligible and does not bias the analysis. The following results present the zonal mean at 65°S; however, the relationships hold over the ice-covered region. With the exception of the dependence of ice thickness on surface air temperature in GFDL-ESM2G, all of the regressions presented below are significant at the 95% level.

[55] The dependence of ice thickness on surface air temperature (Figure 10a) demonstrates that ice thickness decreases as the surface air temperature warms. The strength of the relationship is strongly model dependent, with the ice loss in response to 1°C of warming varying between ~18 cm (NorESM1-M) and ~1 cm (IPSL-CM5A-LR/CanESM2). The relationship between ice thickness and heat storage at depth, represented here by change in potential temperature over a fixed volume, is shown in Figure 10b. With the exception of CSIRO-Mk3–6-0, increases in heat storage at depth occur in conjunction with increasing ice thickness. This relationship is consistent with the key role of entrainment surmised from the estimates of contributions to the salinity and heat budgets above: a weakening of entrainment is associated with increased stratification, decreased convection and thus a decrease in upwelled oceanic heat (and, by inference, increased heat storage at depth). This decrease in upwelled heat thus promotes cooling of the mixed layer, resulting in conditions that are more favorable for ice growth. As for the surface air temperature / ice thickness relationship, however, the relative importance of this process varies dramatically from model to model. CSIRO-Mk3–6-0 does not demonstrate the relationship at all, showing rather a decrease in ice thickness with increased temperature at depth corresponding to the strong increase in temperature evident throughout the top 1000 m of the water column in the zonal mean at this latitude. NorESM1-M and IPSL-CM5A-LR exhibit a strong dependency on heat storage at depth, showing an equivalent change of ~10 cm of ice thickness per 1°C of temperature change at depth, whilst for MPI-ESM-LR and CanESM2, the relationship is almost negligible. The dependency of this relationship on entrainment processes is depicted in Figure 10c, which suggests that the models with the strongest relationship between heat storage at depth and change in ice thickness are also the ones with the largest change in entrainment (as for the initial mixed layer analysis, MPI-ESM-LR is excluded due to the unrealistic entrainment velocities associated with the full-column convection evident in this model). Whilst the small sample size and large discrepancies amongst the models make it impossible to quantify a robust dependency between ice thickness, heat storage at depth and entrainment rate, this exploratory analysis hints that the representation of entrainment may be important in determining the relationship between heat storage at depth and ice thickness.

[56] The Southern Ocean has been shown to have freshened over recent decades, both regionally and at larger scales [e.g., *Jacobs and Giulivi*, 2010; *Durack and Wijffels*, 2010]. Concurrently, Antarctic sea ice extent has been observed to increase slightly over the satellite era [e.g., *Zwally et al.*, 2002; *Comiso and Nishio*, 2008]. This recent change is consistent with the mechanisms hypothesized to exert significant control over sea ice variability, on the condition that the heat supplied by the atmosphere in recent decades has been less than that simulated in the model experiments analyzed here (or that there has been a greater suppression of upwelled oceanic heat). This condition is necessary because the majority of the models studied in

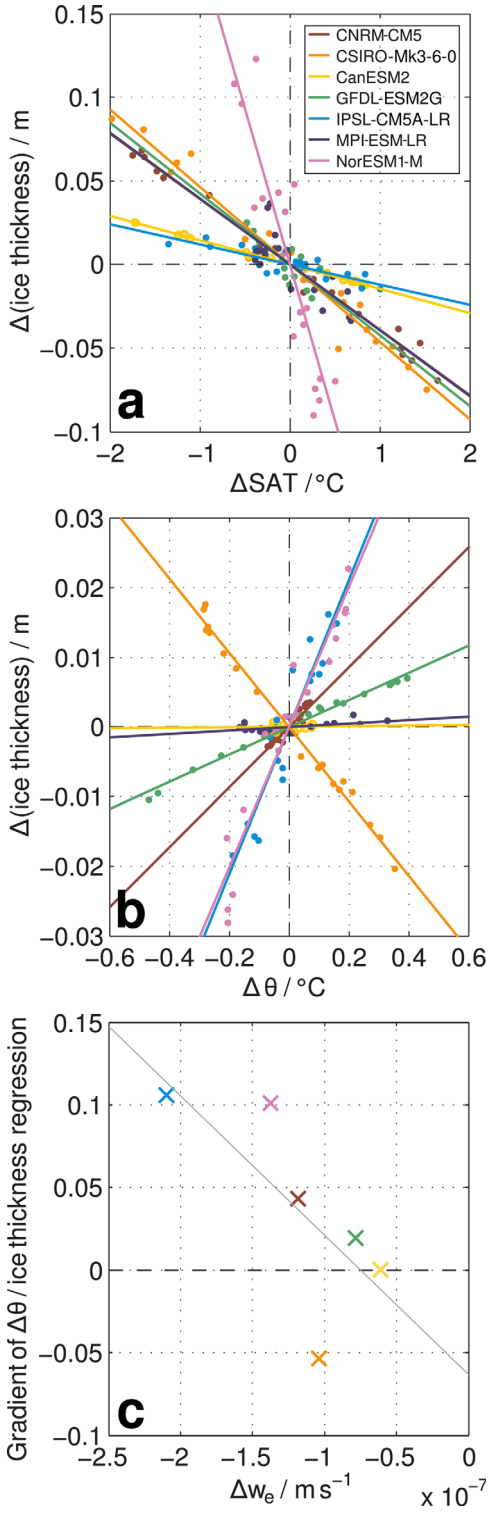

Figure 10. Change in reconstructed zonal-mean sea ice thickness at 65°S derived from multiple-linear regression between sea ice thickness and (a) surface air temperature and (b) mean potential temperature over the depth range 500–1000 m. Colored dots show pentannual averages (see text). (c) Dependence of the strength of the relationship between potential temperature at depth and ice thickness on entrainment. The gray line shows the linear regression of change in entrainment rate on the gradient of the ice thickness / potential temperature regression.

this analysis exhibit strong decreases in sea ice coverage in response to the RCP4.5 forcing scenario, contrasting with the slight increases in sea ice coverage observed since the start of the satellite era. The relatively strong increases in atmospheric heat flux simulated by the models suggest that this condition is plausible. (Further, as noted above, the climate system is complex, and it is likely that mechanisms additional to those considered here are also important in driving both sea ice and oceanic change. Additional climatic forcing mechanisms, such as changes in wind stress, may hence also play a significant role in driving the sea ice loss simulated by the models.) Accurate quantification of both air-sea heat fluxes and recent changes in ocean heat storage and stratification in the high-latitude Southern Ocean will be critical to assessing the importance of entrainment in driving recent observed change.

5. Conclusions

[57] The CMIP5 models analyzed in this work demonstrate a robust and widespread freshening tendency in the RCP4.5 scenario, with an associated decoupling of the mixed layer, which gains buoyancy at a faster rate than the underlying ocean due to the decreasing salinity. In the ice-covered area, there is little change in temperature evident in the upper ocean. However, outside this area the mixed layer temperature increases substantially. With the exception of one model (GFDL-ESM2G), all models simulate an overall decrease in sea ice volume over the 100 year run.

[58] Our evaluation of the terms of the salinity budget and their correlation with mixed layer salinity suggests that the dominant contributions to the simulated freshening are supplied by entrainment and the meltwater input/brine rejection associated with sea ice formation. The vertical distribution of salinity change supports this hypothesis, with the freshening signal being strongest adjacent to the continent and weakening as the anomaly is advected northward and subducted into the ocean interior. However, considering the interdependent nature of the various mechanisms that affect the salinity budget, a potentially crucial role must also be played by atmospheric warming, freshwater input from sea ice melt and/or the evaporation-precipitation balance in initiating the decreases in entrainment rate that are inferred to amplify the (comparatively weaker) initial forcing.

[59] The heat budget analysis presented here suggests that, at large spatial scales, the mixed layer heat content is determined by a balance between the heat supplied by the atmosphere and the entrainment-modulated supply of heat by the ocean underlying the mixed layer. We have proposed in this work that this balance may also be a primary factor in determining sea ice coverage, and that the disparity amongst model representations of the relative importance of these two supplies of heat (and, essentially, the strength of entrainment) may be a key factor in determining the models' differing sea ice distributions. It is not clear at present what the relative strengths of these relationships should be in reality; however, this may be a key issue to resolve. Finally, these results suggest that ocean stratification is a key factor in determining mixed layer heat content, and improved quantification of the magnitude of air-sea heat fluxes and interannual to interdecadal-scale changes in ocean stratification, particularly in the seasonally ice-

covered region, would thus be of great value in understanding recent variability both in the oceanic mixed layer and also in Southern Ocean sea ice coverage.

[60] **Acknowledgments.** We acknowledge the World Climate Research Programme's Working Group on Coupled Modeling, which is responsible for CMIP, and thank the climate modeling groups listed in Table 1 for producing and making available their model output. For CMIP the U.S. Department of Energy's Program for Climate Model Diagnosis and Intercomparison provides coordinating support and led development of software infrastructure in partnership with the Global Organization for Earth System Science Portals. H.G. is a Senior Research Associate with the Fonds National de la Recherche Scientifique (FRS-FNRS-Belgium). This work is supported by the FRS-FNRS and by the Belgian Federal Science Policy Office (Research Program on Science for a Sustainable Development). Computational resources have been provided by the supercomputing facilities of the Université catholique de Louvain (CISM/UCL) and the Consortium des Equipements de Calcul Intensif en Fédération Wallonie Bruxelles (CECI) funded by the Fonds de la Recherche Scientifique de Belgique (F.R.S.-FNRS). We are grateful to two anonymous reviewers for their helpful comments on the manuscript.

References

Bitz, C. M., P. R. Gent, R. A. Woodgate, M. M. Holland, and R. Lindsay (2006), The influence of sea ice on ocean heat uptake in response to increasing CO2, *J. Clim.*, *19*(11), 2437–2450, doi:10.1175/JCLI3756.1.

Böning, C. W., A. Dispert, M. Visbeck, S. R. Rintoul, and F. U. Schwarzkopf (2008), The response of the Antarctic circumpolar current to recent climate change, *Nat. Geosci.*, *1*(12), 864–869, doi:10.1038/ngeo362.

Capotondi, A., M. A. Alexander, N. A. Bond, E. N. Curchitser, and J. D. Scott (2012), Enhanced upper ocean stratification with climate change in the CMIP3 models, *J. Geophys. Res.*, *117*, C04031, doi:10.1029/2011JC007409.

Cavalieri, D., C. Parkinson, P. Gloersen, and H. J. Zwally (1996), *Sea Ice Concentrations from Nimbus-7 SMMR and DMSP SSM/I Passive Microwave Data [1978–2007], Version 1.0.*, Natl. Snow and Ice Data Cent., Boulder, Colo. [updated 2008].

Comiso, J. C. (2002), A rapidly declining perennial sea ice cover in the Arctic, *Geophys. Res. Lett.*, *29*(20), 1956, doi:10.1029/2002GL015650.

Comiso, J. C. (2012), Large decadal decline of the arctic multiyear ice cover, *J. Clim.*, *25*(4), 1176–1193, doi:10.1175/JCLI-D-11–00113.1.

Comiso, J. C., and F. Nishio (2008), Trends in the sea ice cover using enhanced and compatible AMSR-E, SSM/I, and SMMR data, *J. Geophys. Res.*, *113*, C02S07, doi:10.1029/2007JC004257.

Comiso, J. C., R. Kwok, S. Martin, and A. L. Gordon (2011), Variability and trends in sea ice extent and ice production in the Ross Sea, *J. Geophys. Res.*, *116*, C04021, doi:10.1029/2010JC006391.

de Boyer Montégut, C., G. Madec, A. S. Fischer, A. Lazar, and D. Iudicone (2004), Mixed layer depth over the global ocean: An examination of profile data and a profile-based climatology, *J. Geophys. Res.*, *109*, C12003, doi:10.1029/2004JC002378.

Dong, S., S. T. Gille, and J. Sprintall (2007), An assessment of the southern ocean mixed layer heat budget, *J. Clim.*, *20*(17), 4425–4442, doi:10.1175/JCLI4259.1.

Dong, S., S. L. Garzoli, and M. Baringer (2009), An assessment of the seasonal mixed layer salinity budget in the Southern Ocean, *J. Geophys. Res.*, *114*, C12001, doi:10.1029/2008jc005258.

Durack, P. J., and S. E. Wijffels (2010), Fifty-year trends in global ocean salinities and their relationship to broad-scale warming, *J. Clim.*, *23*(16), 4342–4362, doi:10.1175/2010jcli3377.1.

Fahrbach, E., M. Hoppema, G. Rohardt, O. Boebel, O. Klatt, and A. Wisotzki (2011), Warming of deep and abyssal water masses along the Greenwich meridian on decadal time scales: The Weddell gyre as a heat buffer, *Deep Sea Res. Part II*, *58*(25–26), 2509–2523, doi:10.1016/j.dsr2.2011.06.007.

Gille, S. T. (2002), Warming of the Southern Ocean since the 1950s, *Science*, *295*, 1275–1277, doi:10.1126/science.1065863.

Gille, S. T. (2008), Decadal-scale temperature trends in the Southern Hemisphere Ocean, *J. Clim.*, *21*, 4749–4765, doi:10.1175/2008JCLI2131.1.

Gough, A. J., A. R. Mahoney, P. J. Langhorne, M. J. M. Williams, and T. G. Haskell (2012), Sea ice salinity and structure: A winter time series of salinity and its distribution, *J. Geophys. Res.*, *117*, C03008, doi:10.1029/2011JC007527.

Gregory, J. M. (2000), Vertical heat transports in the ocean and their effect on time-dependent climate change, *Clim. Dyn.*, *16*, 501–515, doi:10.1007/s003820000059.

Holland, P. R., and R. Kwok (2012), Wind-driven trends in Antarctic sea-ice drift, *Nat. Geosci.*, *5*, 872–875, doi:10.1038/ngeo1627.

Huang, B., P. H. Stone, A. P. Sokolov, and I. V. Kamenkovich (2003), The deep-ocean heat uptake in transient climate change, *J. Clim.*, *16*(9), 1352–1363, doi:10.1175/1520-0442-16.9.1352.

Jacobs, S. S., and J. C. Comiso (1997), Climate variability in the Amundsen and Bellingshausen Seas, *J. Clim.*, *10*(4), 697–709, doi:10.1175/1520-0442(1997)010 <0697:CVITAA >2.0.CO;2.

Jacobs, S. S., and C. F. Giulivi (2010), Large multidecadal salinity trends near the Pacific–Antarctic continental margin, *J. Clim.*, *23*(17), 4508–4524, doi:10.1175/2010JCLI3284.1.

Jacobs, S. S., C. F. Giulivi, and P. A. Mele (2002), Freshening of the Ross Sea during the late 20th century, *Science*, *297*(5580), 386–389, doi:10.1126/science.1069574.

Liu, J., and J. A. Curry (2010), Accelerated warming of the Southern Ocean and its impacts on the hydrological cycle and sea ice, *Proc. Natl. Acad. Sci. U. S. A.*, *107*(34), 14,987–14,992, doi:10.1073/pnas.1003336107.

Liu, J., J. A. Curry, and D. G. Martinson (2004), Interpretation of recent Antarctic sea ice variability, *Geophys. Res. Lett.*, *31*, L02205, doi:10.1029/2003gl018732.

Manabe, S., R. J. Stouffer, M. J. Spelman, and K. Bryan (1991), Transient responses of a coupled ocean-atmosphere model to gradual changes of atmospheric CO2, Part I: Annual mean response, *J. Clim.*, *4*(8), 785–818, doi:10.1175/1520-0442(1991)004 <0785:TROACO >2.0.CO;2.

Martinson, D. G., S. E. Stammerjohn, R. A. Iannuzzi, R. C. Smith, and M. Vernet (2008), Western Antarctic Peninsula physical oceanography and spatiotemporal variability, *Deep Sea Res. Part II*, *55*(18–19), 1964–1987, doi:10.1016/j.dsr2.2008.04.038.

Parkinson, C. L., and D. J. Cavalieri (2012), Antarctic sea ice variability and trends, 1979–2010, *Cryosphere*, *6*(4), 871–880, doi:10.5194/tc-6–871-2012.

Ren, L., K. Speer, and E. P. Chassignet (2011), The mixed layer salinity budget and sea ice in the Southern Ocean, *J. Geophys. Res.*, *116*, C08031, doi:10.1029/2010JC006634.

Sallée, J.-B., K. Speer, R. Morrow, and R. Lumpkin (2008), An estimate of Lagrangian eddy statistics and diffusion in the mixed layer of the Southern Ocean, *J. Mar. Res.*, *66*(4), 441–463, doi:10.1357/002224008787157458.

Sen Gupta, A., A. Santoso, A. S. Taschetto, C. C. Ummenhofer, J. Trevena, and M. H. England (2009), Projected changes to the Southern Hemisphere Ocean and sea ice in the IPCC AR4 climate models, *J. Clim.*, *22*(11), 3047–3078, doi:10.1175/2008JCLI2827.1.

Simmonds, I., and T. H. Jacka (1995), Relationships between the interannual variability of Antarctic sea ice and the Southern oscillation, *J. Clim.*, *8*(3), 637–647, doi:10.1175/1520-0442(1995)008 <0637:RBTIVO >2.0.CO;2.

Stammerjohn, S., R. Massom, D. Rind, and D. Martinson (2012), Regions of rapid sea ice change: An interhemispheric seasonal comparison, *Geophys. Res. Lett.*, *39*(6), doi:10.1029/2012GL050874.

Stammerjohn, S. E., and R. C. Smith (1997), Opposing Southern Ocean climate patterns as revealed by trends in regional sea ice coverage, *Clim. Change*, *37*(4), 617–639, doi:10.1023/a:1005331731034.

Stammerjohn, S. E., D. G. Martinson, R. C. Smith, X. Yuan, and D. Rind (2008), Trends in Antarctic annual sea ice retreat and advance and their relation to El Niño—Southern oscillation and southern annular mode variability, *J. Geophys. Res.*, *113*, C03S90, doi:10.1029/2007JC004269.

Taylor, K. E., R. J. Stouffer, and G. A. Meehl (2011), An overview of CMIP5 and the experiment design, *Bull. Am. Meteorol. Soc.*, *93*(4), 485–498, doi:10.1175/BAMS-D-11–00094.1.

Turner, J., et al. (2009), Nonannular atmospheric circulation change induced by stratospheric ozone depletion and its role in the recent increase of Antarctic sea ice extent, *Geophys. Res. Lett.*, *36*, L08502, doi:10.1029/2009gl037524.

Watanabe, T., M. Ikeda, and M. Wakatsuchi (2004), Thermohaline effects of the seasonal sea ice cover in the Sea of Okhotsk, *J. Geophys. Res.*, *109*, C09S02, doi:10.1029/2003jc001905.

Yuan, X., and C. Li (2008), Climate modes in southern high latitudes and their impacts on Antarctic sea ice, *J. Geophys. Res.*, *113*, C06S91, doi:10.1029/2006jc004067.

Zhang, J. (2007), Increasing Antarctic sea ice under warming atmospheric and oceanic conditions, *J. Clim.*, *20*(11), 2515–2529, doi:10.1175/JCLI4136.1.

Zwally, H. J., J. C. Comiso, C. L. Parkinson, D. J. Cavalieri, and P. Gloersen (2002), Variability of Antarctic sea ice 1979–1998, *J. Geophys. Res.*, *107*(C5), doi:10.1029/2000jc000733.